JACS
JOURNAL OF THE AMERICAN CHEMICAL SOCIETY

Article

pubs.acs.org/JACS

Singlet–Triplet Splittings in the Luminescent Excited States of Colloidal Cu^+:CdSe, Cu^+:InP, and $CuInS_2$ Nanocrystals: Charge-Transfer Configurations and Self-Trapped Excitons

Kathryn E. Knowles, Heidi D. Nelson, Troy B. Kilburn, and Daniel R. Gamelin*

Department of Chemistry, University of Washington, Seattle, Washington 98195-1700, United States

Supporting Information

ABSTRACT: The electronic and magnetic properties of the luminescent excited states of colloidal Cu^+:CdSe, Cu^+:InP, and $CuInS_2$ nanocrystals were investigated using variable-temperature photoluminescence (PL) and magnetic circularly polarized luminescence (MCPL) spectroscopies. The nanocrystal electronic structures were also investigated by absorption and magnetic circular dichroism (MCD) spectroscopies. By every spectroscopic measure, the luminescent excited states of all three materials are essentially indistinguishable. All three materials show very similar broad PL line widths and large Stokes shifts. All three materials also show similar temperature dependence of their PL lifetimes and MCPL polarization ratios. Analysis shows that this temperature dependence reflects Boltzmann population distributions between luminescent singlet and triplet excited states with average singlet–triplet splittings of ~1 meV in each material. These similarities lead to the conclusion that the PL mechanism in $CuInS_2$ NCs is fundamentally different from that of bulk $CuInS_2$ and instead is the same as that in Cu^+-doped NCs, which are known to luminesce via charge-transfer recombination of conduction-band electrons with copper-localized holes. The luminescence of $CuInS_2$ nanocrystals is explained well by invoking exciton self-trapping, in which delocalized photogenerated holes contract in response to strong vibronic coupling at lattice copper sites to form a luminescent excited state that is essentially identical to that of the Cu^+-doped semiconductor nanocrystals.

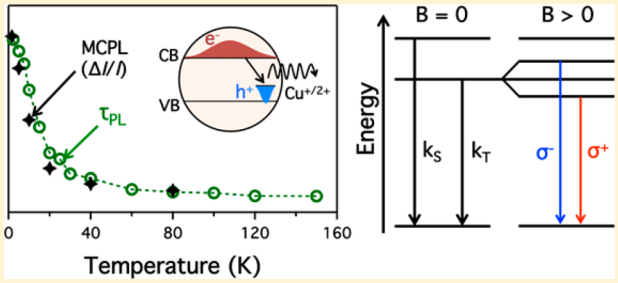

INTRODUCTION

Copper-doped semiconductors are classic phosphor materials that have been used in a variety of applications for nearly a century.[1] Recently, attention has turned to the development of colloidal copper-doped semiconductor nanocrystals (NCs), which combine the unique luminescence properties of copper-doped semiconductors with the solubility and optoelectronic tunability of semiconductor NCs. Ternary semiconductor NCs containing copper as a (formally) stoichiometric component of their composition, for example $CuInS_2$ or $CuInSe_2$, have also recently generated interest as cadmium- and lead-free alternatives to more conventional NC materials, such as CdSe and PbS.[2−7] Both the copper-doped and copper-based NCs have size and composition-tunable energy gaps and display very broad, tunable photoluminescence (PL) bands centered at energies significantly lower than their band gap energies.[2,3,8−11] This tunability, combined with the minimal overlap between their absorption and PL spectra, make such NCs attractive phosphors for numerous applications in optical imaging and spectral conversion.[12−16] For example, we have recently demonstrated that Cu^+:CdSe and $CuInS_2$/CdS core/shell NCs exceed the performance of other leading colloidal NC phosphors when used as luminophores in luminescent solar concentrators.[14,15] To optimize these materials as phosphors, it is important to understand the details of their PL mechanisms, many of which remain largely unexplored. Here, we examine the luminescent excited states of two copper-doped semiconductor NC materials, Cu^+:CdSe and Cu^+:InP, and one copper-based semiconductor NC material, $CuInS_2$, using a combination of temperature-dependent PL and magneto-optical spectroscopies.

Photoluminescence in bulk copper-doped semiconductor phosphors originates from recombination of an electron that is partially localized at a shallow donor defect with a hole that is strongly localized at a deep acceptor level associated with the copper dopant.[1,17] This donor–acceptor pair luminescence is characterized by a long PL decay time dictated by the spatial separation between the donor and acceptor sites, and a PL energy that is determined by the combined depths of the donor and acceptor defects. The PL energy is thus much smaller than the band gap energy of the host semiconductor. Like their bulk counterparts, photoluminescence in copper-doped semiconductor NCs arises from recombination of a largely delocalized electron with a copper-localized hole, but in most cases the electron appears to occupy the NC conduction band (CB) rather than being bound to an individual donor defect. For example, several researchers have observed that the luminescence of copper-doped semiconductor NCs shifts to lower energy as the CB shifts to lower energy due to changes in the

Received: August 12, 2015
Published: September 21, 2015

DOI: 10.1021/jacs.5b08547
J. Am. Chem. Soc. 2015, 137, 13138–13147

NC size or composition.[2,8,9,18−21] These observations establish charge-transfer recombination of a CB electron with a copper-localized hole as the accepted mechanism of PL in copper-doped semiconductor NCs (Figure 1, arrow 3). According to this mechanism, the energy difference between the first excitonic absorption and the PL peaks is determined primarily by the energy difference between the copper 3*d* orbitals and the valence-band (VB) edge. Pronounced delayed luminescence was also recently observed in copper-doped NCs and attributed to electron trapping and detrapping at NC surface sites,[22] analogous to the delayed donor−acceptor luminescence of bulk copper-doped semiconductors.[1,17]

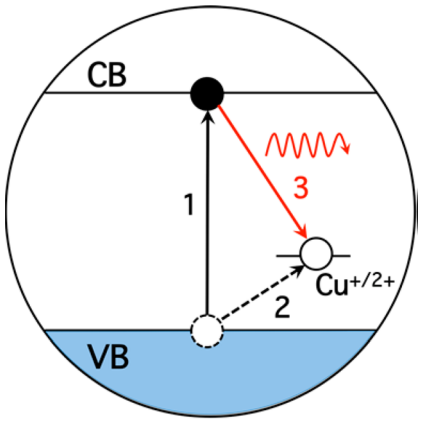

Figure 1. Illustration of the mechanism of $ML_{CB}CT$ luminescence in Cu^+-doped semiconductor nanocrystals. Upon photoexcitation (1), the hole rapidly and nonradiatively localizes from the valence band to a Cu^+ dopant to form a Cu^{2+}-like ion (2). Radiative recombination of the electron from the conduction band with the copper-localized hole results in emission of a photon (3).

The origins of the large PL line widths observed in copper-doped semiconductor NCs are still under debate. Luminescence line narrowing measurements have demonstrated that this line width is not a consequence of size heterogeneity within an ensemble of doped NCs, and this width was instead concluded to arise from a distribution of copper energy levels due to local structural inhomogeneities.[23] PL spectra of single NCs possessing single copper dopants show the same large line width as the ensemble spectrum, suggesting a homogeneous origin.[22] We favor the attribution of this large line width primarily to homogeneous vibronic contributions resulting from the large nuclear reorganization that accompanies excited-state charge separation and hole localization by copper. In support of this interpretation, we note that the PL mechanism described above for copper-doped semiconductor NCs is not only similar to that in bulk copper-doped semiconductor phosphors, but it is also directly analogous to the metal-to-ligand charge transfer (MLCT) luminescence of many tetrahedral Cu^+ coordination compounds that also exhibit broad PL bands.[24−26] The PL line widths in these molecules indeed reflect the formation of a Cu^{2+}-like center in the MLCT excited state and the concomitant nuclear reorganization. In copper-doped semiconductor NCs, the lowest-energy CB orbital plays the same role as the ligand-based lowest unoccupied molecular orbitals (LUMOs) of these molecular MLCT excited states. We therefore refer to the luminescent excited states of copper-doped semiconductor NCs as $ML_{CB}CT$ excited states.

Although there is general consensus that the PL of copper-doped semiconductor NCs involves recombination of a CB electron with a copper-localized hole, there is considerable disagreement in the literature about the origin of this copper-localized hole. This disagreement stems from conflicting reports of the oxidation state of copper in the doped-NC ground state. Most reports claim that copper is in the +1 oxidation state prior to photoexcitation.[19,22,27−32] In this scenario, a photogenerated hole rapidly localizes at a Cu^+ dopant to form a Cu^{2+}-like ion (Figure 1, arrow 2). Recombination of the photogenerated electron with this localized hole then leads to $ML_{CB}CT$ luminescence (Figure 1, arrow 3). Some reports claim that copper is already in the +2 oxidation state prior to photoexcitation.[8,23,33,34] In this scenario, a CB electron generated by photoexcitation across the gap can still recombine with the copper-localized hole to yield $ML_{CB}CT$ luminescence, but this charge-transfer recombination has to compete with direct recombination of the delocalized electron−hole pair, which is an order of magnitude faster. Enhancement of the copper-based PL upon addition of ligands known to trap VB holes has been interpreted in terms of elimination of this competing excitonic recombination channel.[34] The process allowing copper-based holes to be regenerated after radiative $ML_{CB}CT$ recombination in this scenario has not been described.

Despite these remaining ambiguities, the PL of copper-doped semiconductor NCs is still much better understood than that of $CuInS_2$ NCs (and related NCs). Bulk $CuInS_2$ shows a characteristic deep-trap luminescence that has been linked to specific point defects, namely Cu_{In}, V_{In}, and V_{Cu}.[35,36] The PL of $CuInS_2$ NCs is almost universally attributed to similar point defects, but the identities of these defects remain unclear.[3,5,16,37−41] For example, the broad luminescence of $CuInS_2$ NCs has been attributed to recombination of CB electrons with holes localized at defects.[3,16,41] This mechanism is similar to that of copper-doped semiconductor NCs in that it invokes recombination of CB electrons with localized holes, but the hole traps are not identified. A recent report has described similar magnetic circularly polarized luminescence (MCPL) field dependence between 0 and 1 T at 3 K in $CuInS_2$ and copper-doped ZnSe NCs.[42] These MCPL data were interpreted as indicating that Cu^{2+} plays an essential role in the ground states of both the $CuInS_2$ and copper-doped ZnSe NCs.

Here, we report a detailed investigation of the PL and magneto-PL of Cu^+:CdSe, Cu^+:InP, and $CuInS_2$ NCs aimed at clarifying the electronic structures of these materials in their ground and luminescent excited states. These three NCs all display similar PL line widths and Stokes shifts. Magnetic circular dichroism (MCD) measurements demonstrate that these NCs are diamagnetic in their ground states, consistent with copper in the +1 oxidation state. Variable-temperature PL measurements reveal large increases in the PL decay times of all three materials as the temperature is lowered below ∼60 K. These data are interpreted in terms of singlet−triplet splittings within luminescent $ML_{CB}CT$ excited states of all three types of NCs, arising from magnetic-exchange coupling of delocalized CB electron spins with localized Cu(3*d*) spins. Quantitative analysis yields very similar average singlet−triplet splitting energies for each of these three NC materials (∼1 meV). This interpretation of the temperature dependence of the PL lifetimes is confirmed by variable-temperature MCPL measurements performed up to 6 T and up to 80 K. The MCPL polarization ratios of $CuInS_2$, Cu^+:CdSe, and Cu^+:InP NCs are

DOI: 10.1021/jacs.5b08547
J. Am. Chem. Soc. 2015, 137, 13138−13147

similar at all fields and temperatures. MCPL selectively probes the triplet $ML_{CB}CT$ emission, providing an independent and model-free measurement of the triplet state's temperature-dependent Boltzmann population that coincides well with that determined from PL lifetimes. The spectroscopic data for all three types of NCs are thus explained thoroughly without invoking the presence of Cu^{2+} in the ground state.

Because every spectroscopic result presented here for the $CuInS_2$ NCs is essentially indistinguishable from the analogous result obtained for the Cu^+-doped NCs, we propose that the PL mechanism in $CuInS_2$ NCs is fundamentally the same as the one illustrated in Figure 1: photoexcitation (arrow 1) is followed by rapid hole localization around an individual Cu^+ to form a Cu^{2+}-like ion (arrow 2), followed by radiative $ML_{CB}CT$ recombination of this copper-localized hole with the delocalized CB electron (arrow 3). A new interpretation of the PL mechanism of $CuInS_2$ NCs is thus proposed, namely exciton self-trapping.[43−46] This interpretation differs from previous interpretations in that exciton self-trapping requires no point defects, but instead requires only intrinsically strong electron−phonon coupling in the photoexcited state. This condition is met in the $CuInS_2$ NCs. The details and implications of this new interpretation of $CuInS_2$ NC PL are discussed.

EXPERIMENTAL METHODS

Synthesis of Cu^+:CdSe Nanocrystals. We adapted a literature procedure for the synthesis of Cu^+:CdSe NCs by hot injection.[47] Cadmium acetate hydrate (0.116 g, 0.5 mmol), oleic acid (0.32 g, 1.1 mmol), and hexadecane (5 g) were degassed under vacuum at 70 °C for 1 h. Heating the mixture to 110 °C under nitrogen for 10 min produced a clear, colorless solution. After cooling to 70 °C, copper stearate (0.032 g, 0.05 mmol) was added under positive nitrogen flow, the mixture was degassed with three pump-purge cycles at 70 °C, and then the temperature was increased to 180 °C under nitrogen. Rapid injection of 0.25 mL of a 1 M solution of selenium in trioctylphosphine at 180 °C caused the mixture to change color from deep blue to colorless to red within 1 min. After 30 min at 180 °C, the mixture was cooled to room temperature. Addition of an equal volume of a ∼ 3:1 ethanol:acetone mixture followed by centrifugation produced dark red pellets from a colorless supernatant. The supernatant was discarded, and the pellets were washed with acetone, dried under nitrogen flow, and redispersed in toluene.

Synthesis of Cu^+:InP Nanocrystals. The procedure for synthesis of Cu^+:InP NCs was adapted from ref 9. Indium acetate (0.117 g, 0.4 mmol), myristic acid (0.292 g, 1.28 mmol), and octadecene (4 g) were degassed under vacuum at 100 °C for 2 h and then heated to 300 °C. Rapid injection of a solution of tris(trimethylsilyl) phosphine (58 μL, 0.2 mmol) in octadecene (2.5 mL) resulted in a color change from colorless to red to dark brown. After 30 min at 300 °C, the mixture was cooled to 100 °C, and a solution of copper stearate (0.025 g, 0.04 mmol) in octadecene (4 g) was added dropwise. The mixture was heated to 220 °C over 1.5 h and then cooled to room temperature. The Cu^+:InP cores formed at this point exhibit very weak luminescence (quantum yield ∼1.5%), consistent with literature results.[9] Growth of a very thin $ZnSe_{1-x}S_x$ alloy shell following literature procedures increased the quantum yield to up to 24% without changing the absorption or PL spectra (see Supporting Information).

Synthesis of $CuInS_2$ Nanocrystals. We adapted a literature procedure for the synthesis of $CuInS_2$ NCs.[3] Indium acetate (0.294 g, 1 mmol), copper iodide (0.191 g, 1 mmol), and dodecanethiol (5 mL) were added to a 50 mL three-neck round-bottom flask. The flask was degassed with three pump-purge cycles using nitrogen at room temperature. After the last cycle, the reaction mixture was heated at 100 °C under nitrogen for 10 min during which it transforms into an optically clear pale yellow solution. The temperature was then increased to 230 °C. When the temperature became greater than 200 °C the color of the solution began to change from yellow to orange to dark red. After 10 min at 220 °C, the mixture became dark black in color and was rapidly cooled to 60 °C using a water bath. At 60 °C, the reaction was opened to air, and ∼2 mL of toluene and ∼1 mL oleic acid were added. The mixture was stirred for 20 min at 60 °C, then cooled to room temperature. The NCs were purified by precipitation with ethanol, followed by centrifugation and resuspension in toluene.

Spectroscopic Methods. Absorption spectra of toluene solutions of Cu^+:CdSe, Cu^+:InP, and $CuInS_2$ nanocrystals were measured on a Varian Cary 500 spectrometer, and solution-phase PL spectra were measured using an Ocean Optics USB-2000+ spectrometer with perpendicular 405 nm excitation. All PL spectra were corrected for the instrument response. PL quantum yields were measured in toluene solution at room temperature using an integrating sphere. NC compositions were determined by inductively coupled plasma atomic emission spectroscopy (ICP-AES, see Supporting Information for details).

Temperature-dependent PL measurements were performed on films of nanocrystals sandwiched between circular quartz plates. The films were loaded into an Oxford SM-2 cryostat. A 405 nm diode laser was used for photoexcitation at an incident angle of ∼10−15° relative to the optical detection axis. Excitation was modulated at 100 Hz with the square wave output from a function generator. The PL was passed through a 420 nm long-pass filter and focused into a monochromator (0.5 m, 150 g/mm grating blazed at 500 nm) equipped with a photomultiplier tube (PMT) connected to a multichannel scaler. Several thousand excitation pulses were averaged to measure PL decay kinetics. The time resolution of this apparatus is 5 ns. PL lifetime measurements were performed without an applied magnetic field.

For magnetic circularly polarized luminescence (MCPL) measurements, nanocrystal films were loaded into a superconducting magneto-optical cryostat with a variable-temperature sample compartment (Cryo-Industries SMC-1659 OVT). Continuous 405 nm excitation was used. PL was collected along the magnetic field axis (Faraday geometry), passed through a liquid crystal variable retardation plate set to $\lambda/4$ at the emission maximum, followed by a linear polarizer used to separate left and right circularly polarized PL components. A 420 nm long-pass filter placed after the linear polarizer removed scattered excitation light before the PL was collected by an optical fiber and directed into the same monochromator, which dispersed the PL onto a liquid-nitrogen-cooled charge-coupled device (CCD). MCPL polarization ratios were then calculated from the relative intensities of left and right circularly polarized PL at various applied magnetic field strengths, following the sign convention described in Piepho and Schatz.[48]

RESULTS

1. Nanocrystal Characterization. Figure 2 shows absorption and photoluminescence spectra of three different nanocrystal samples: Cu^+:CdSe NCs with a Cu:Cd ratio of 0.0061 ± 0.0001, Cu^+:InP with a Cu:In ratio of 0.031 ± 0.001, and stoichiometric $CuInS_2$ NCs with Cu:In ratio of 0.98 ± 0.02. Powder X-ray diffraction (p-XRD) measurements confirm that the crystal structures of all three samples are consistent with those of the corresponding undoped bulk materials (see Supporting Information). The absorption spectra of the Cu^+:CdSe and Cu^+:InP NCs show clear excitonic features at 2.23 and 2.30 eV, which correspond to average diameters of 3.2 and 2.9 nm, respectively.[49,50] The absorption spectrum of the $CuInS_2$ NCs exhibits a broad shoulder at ∼2.2 eV, characteristic of NCs with diameters ∼3 nm.[3,11] These sizes are consistent with those estimated from Scherrer analysis of the p-XRD line widths, except in the case of Cu^+:InP, for which the Scherrer analysis yields a smaller diameter (∼2 nm vs 2.9 nm), perhaps due to alloying upon $ZnSe_{1-x}S_x$ shell growth (see Supporting Information). Each sample shows a broad luminescence band

DOI: 10.1021/jacs.5b08547
J. Am. Chem. Soc. 2015, 137, 13138−13147

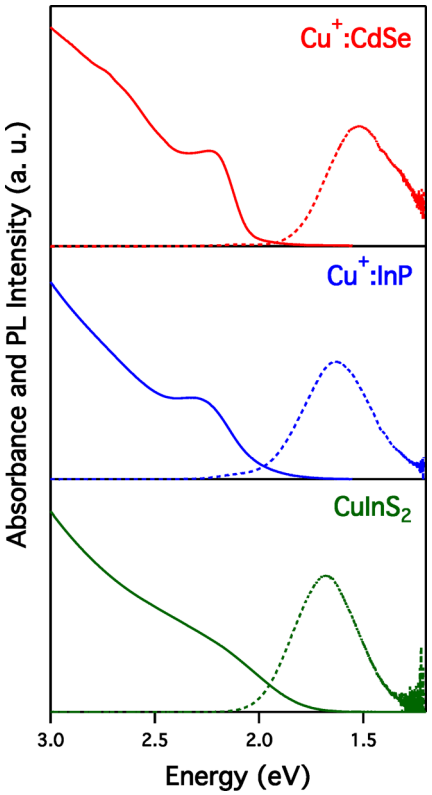

Figure 2. Electronic absorption (solid) and photoluminescence (dashed) spectra of toluene solutions of Cu^+:CdSe (red, $d \sim 3.2$ nm, 0.6% Cu^+), Cu^+:InP (blue, $d \sim 2.9$ nm, 3% Cu^+), and $CuInS_2$ (green, $d \sim 2.7$ nm) nanocrystals taken at room temperature.

centered near 1.6 eV with a full width at half-maximum (fwhm) around 370 meV (see Table 1). The small PL intensities observed to higher energy in the PL spectra of the Cu^+:CdSe and Cu^+:InP NCs are attributable to excitonic PL originating from small subsets of undoped NCs in each sample, as confirmed by the absence of excitonic PL in the spectra of individual copper-doped CdSe NCs.[22] The PL quantum yields (QYs) of these samples are also listed in Table 1 and are all very similar (~0.23). Magnetic circular dichroism (MCD) spectra collected in the visible and near-infrared regions at various temperatures and applied magnetic fields show no evidence of Cu^{2+} in the ground states of any of the NCs of Figure 2 (see Supporting Information). We therefore conclude that the ground states of all of the samples shown in Figure 1 contain copper exclusively in its +1 (diamagnetic) oxidation state.

For the Cu^+:CdSe and Cu^+:InP NCs, the broad PL line width and large separation between the energies of the absorption and PL peaks (i.e., the apparent Stokes shift) are both characteristic of the established $ML_{CB}CT$ PL mechanism described in Figure 1. These PL spectra do not change substantially upon cooling to liquid-helium temperatures (see Supporting Information). Both of these features—broad PL line width and large apparent Stokes shift—are also observed in the PL spectrum of the $CuInS_2$ NCs (Figure 2).

The Cu^+:CdSe and Cu^+:InP NCs both display a weak and broad absorption "foot" that tails to lower energy below the first excitonic absorption peak (Figure 3). This foot is interpreted as the $ML_{CB}CT$ absorption that directly forms the luminescent excited state. The same broad absorption foot is observed in bulk Cu^+-doped II–VI semiconductors.[17] The per-copper extinction coefficient of this foot is $\varepsilon_{Cu} < 1000\ M_{Cu}^{-1}\ cm^{-1}$ at its maximum, consistent with assignment of this absorption to an $ML_{CB}CT$ transition. With this assignment, the actual PL Stokes shifts of the doped NCs are understood to be smaller than the apparent Stokes shifts listed in Table 1. Estimating the center of this absorption foot in the Cu^+:CdSe and Cu^+:InP NCs as the position of the lowest-energy extremum in the second derivatives of the spectra shown in Figure 2 allows estimation of the actual Stokes shifts, listed in Table 1. The differences between these values are close to the uncertainty in the locations of the absorption positions, and are therefore not significant. The quantitative similarities in actual Stokes shifts and in PL line widths between the Cu^+-doped and $CuInS_2$ NCs (Table 1) suggests that the PL mechanisms in these NCs may be similar. Interestingly, the broad lowest-energy feature of the $CuInS_2$ NC absorption spectrum also has a per-copper extinction coefficient of $\varepsilon_{Cu} < 1000\ M_{Cu}^{-1}\ cm^{-1}$ (Figure 3). The sub-bandgap absorption foot of the copper-doped NCs thus appears to be the dilute analog of the first absorption feature in the $CuInS_2$ NCs.

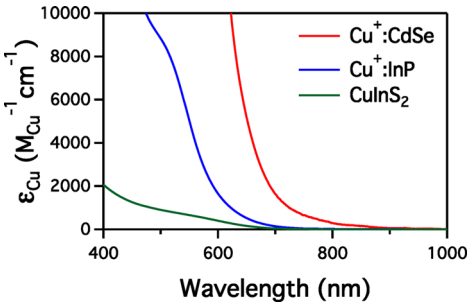

Figure 3. Room-temperature absorption spectra of Cu^+:CdSe (red), Cu^+:InP (blue), and $CuInS_2$ (green) nanocrystals, with intensities plotted in units of per-copper extinction coefficient, ε_{Cu} ($M_{Cu}^{-1}\ cm^{-1}$).

Table 1. Absorption and PL Spectral Parameters for Copper-Containing Nanocrystals

sample	abs. peak position (eV)	PL peak position (eV)	apparent Stokes shift (eV)	est. actual Stokes shift (eV)	fwhm of PL (meV)	PL QY
Cu^+:CdSe	2.23	1.52	0.71	0.55	400	0.25
Cu^+:InP	2.30	1.63	0.67	0.46	390	0.24
$CuInS_2$	~2.2	1.68	~0.5	~0.5	360	0.22

2. Temperature Dependence of Excited-State Lifetimes. Figure 4A plots PL decay kinetics between $t = 0$ and 10 μs for the same Cu^+:CdSe, Cu^+:InP, and $CuInS_2$ NCs as shown in Figure 2 at selected temperatures between 2 and 150 K, normalized at $t = 0$ μs. At low temperatures, the PL of the Cu^+:CdSe NCs decays faster than that of both the Cu^+:InP and $CuInS_2$ NCs, but the temperature dependence of the PL decay in all three samples exhibits the same general behavior. In each case, the decay accelerates markedly when the temperature is raised from 2 to ~60 K, and it becomes temperature-independent above ~60 K. These main qualitative features are evident from visual inspection of the PL decay traces in Figure 4A. The decay data can be fitted in multiple ways to extract quantitative details, but the specific fitting function has only a minor impact on the results. Here, the Cu^+:CdSe NC PL decay traces were fit to single-exponential functions over a 10-

DOI: 10.1021/jacs.5b08547
J. Am. Chem. Soc. 2015, 137, 13138–13147

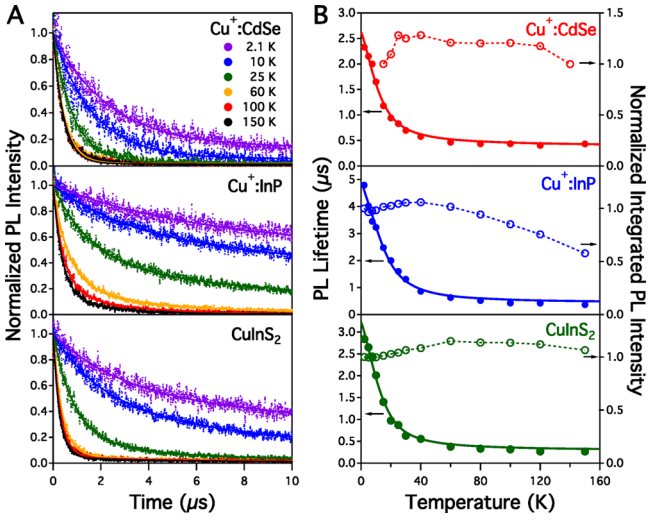

Figure 4. (A) Photoluminescence decay traces measured at the peak of the PL spectrum for Cu^+:CdSe (top), Cu^+:InP (middle), and $CuInS_2$ (bottom) NCs at selected temperatures between 2 and 150 K, normalized at $t = 0$ μs. The solid lines represent fits of the data to a single-exponential function over a 10 μs window for the Cu^+:CdSe NCs and a biexponential function over a 160 μs window for the Cu^+:InP and $CuInS_2$ NCs. (B) PL lifetimes (closed circles, left axis) and normalized spectrally integrated PL intensities (open circles, right axis) of Cu^+:CdSe (top, red), Cu^+:InP (middle, blue), and $CuInS_2$ (bottom, green) NCs plotted versus temperature. The Cu^+:InP and $CuInS_2$ NC lifetimes represent the short-time components of the biexponential fits. Essentially indistinguishable results are obtained from other approaches to fitting the PL decay curves. The solid lines in (B) show fits of the lifetime data to eq 3, and the dashed lines are guides to the eye.

μs window. The PL decay traces of the Cu^+:InP and $CuInS_2$ NCs do not fit well to single-exponential functions (see Supporting Information), and were fit instead to biexponential functions over a 160-μs window to account for decay components with time constants greater than 10 μs. These longer components have especially significant amplitudes at the lower temperatures. We restrict our fits to these time windows (10 μs for Cu^+:CdSe and 160 μs for Cu^+:InP and $CuInS_2$) because (i) for each sample, over 80% of the total PL amplitude decays within these windows at all temperatures, and (ii) the PL decay traces for Cu^+:InP and $CuInS_2$ are highly nonexponential over longer time windows. We have recently reported pronounced delayed luminescence in Cu^+:CdSe NCs associated with reversible trapping of CB electrons.[22] Very similar delayed PL is also observed here in the Cu^+:InP and $CuInS_2$ NCs, and will be discussed in detail in a later paper.

Figure 4B plots the PL lifetimes of the Cu^+:CdSe, Cu^+:InP, and $CuInS_2$ NCs obtained from the traces in Figure 4A versus temperature. All three samples show a steep decrease in the PL lifetime as the temperature increases from 2 to ~60 K, and almost no change in PL lifetime as the temperature increases from 60 to 150 K. The PL lifetimes of all three samples remain fairly constant as the temperature increases from 150 K to room temperature (see Supporting Information). Figure 4B also plots the temperature dependence of the spectrally integrated PL intensity normalized to the intensity measured at the lowest temperature for which spectra were acquired. The PL intensity for each sample increases slightly over the same temperature range where the lifetime decreases (2–60 K). For temperatures from 60 to 150 K, the PL intensities of both the Cu^+:CdSe and $CuInS_2$ NCs remain fairly constant, whereas the PL intensity of the Cu^+:InP NCs decreases slowly with increasing temperature.

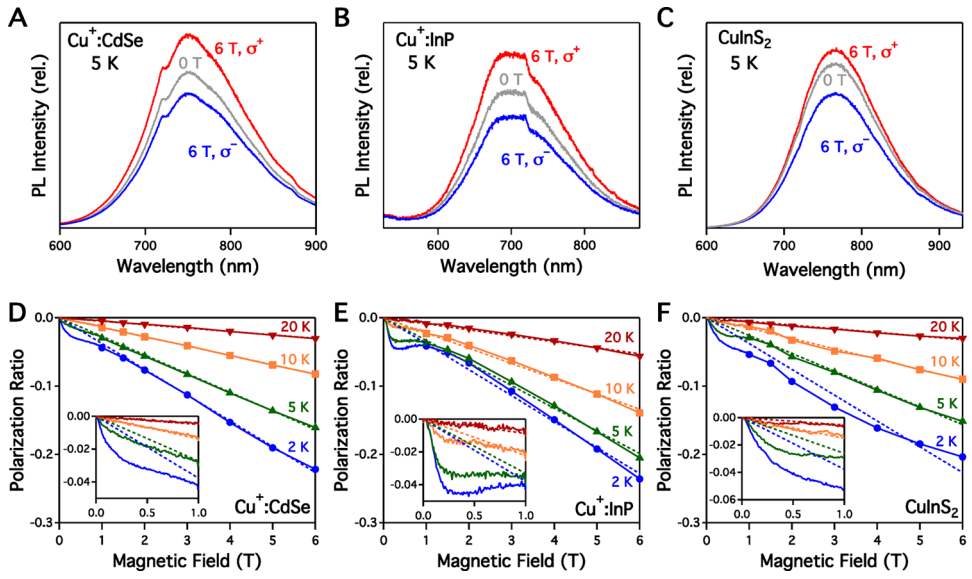

Figure 5. Top: Circularly polarized photoluminescence spectra of (A) Cu^+:CdSe, (B) Cu^+:InP, and (C) $CuInS_2$ nanocrystals measured at 5 K with applied magnetic fields of 0 (gray) and 6 T (blue: left circularly polarized, σ^-; red: right circularly polarized, σ^+). The sharp feature at 730 nm in the Cu^+:CdSe and Cu^+:InP spectra corresponds to absorption from the optical fiber that was not completely eliminated by spectral correction. Bottom: MCPL polarization ratio ($\Delta I/I$) measured at the peak of the zero-field PL spectrum plotted versus applied magnetic field at 2 (blue), 5 (green), 10 (orange), and 20 K (maroon) for (D) Cu^+:CdSe, (E) Cu^+:InP, and (F) $CuInS_2$ nanocrystals. The insets to (D–F) plot the same data from 0 to 1 T. The dashed lines show linear fits of the data from 1 to 6 T with the y-intercept fixed at zero. The Cu^+:CdSe and Cu^+:InP NCs are the same as in Figures 2 and 4, and the $CuInS_2$ NCs are from a different synthetic batch but are spectroscopically nearly identical to those shown in Figures 2 and 4 (see Supporting Information).

DOI: 10.1021/jacs.5b08547
J. Am. Chem. Soc. 2015, 137, 13138–13147

In addition to similar PL lineshapes and apparent Stokes shifts, the data in Figure 4 clearly demonstrate that the PL lifetimes of the Cu^+-doped and $CuInS_2$ NCs all show the same characteristic temperature dependence. This observation is a strong indication that the underlying mechanism of PL in all three of these materials is the same.

3. Magnetoluminescence. The $ML_{CB}CT$ PL mechanism described in Figure 1 can be viewed as involving emission from an excited state that contains a paramagnetic Cu^{2+}-like ion exchange coupled to a CB electron. We have therefore used magnetic circularly polarized luminescence (MCPL) spectroscopy to probe the luminescent excited states of our Cu^+-doped and $CuInS_2$ NCs. Figure 5 summarizes the MCPL data collected for these NCs. Figure 5A−C plots circularly polarized PL spectra measured at 5 K for Cu^+:CdSe, Cu^+:InP, and $CuInS_2$ NCs, respectively, at 0 and 6 T. Under an applied magnetic field, the intensity of right circularly polarized luminescence (σ^+) increases and that of left circularly polarized luminescence (σ^-) decreases. These changes are attributed to a Zeeman splitting of the luminescent excited state that decreases the energy of a σ^+-emitting sublevel and increases the energy of a σ^--emitting sublevel, thereby increasing the Boltzmann population of the former relative to the latter at low temperatures and large applied magnetic fields.

Eq 1 defines the MCPL polarization ratio, $\Delta I/I$, as the difference between left and right circularly polarized PL intensities divided by their sum. Figure 5D−F plots $\Delta I/I$ versus applied magnetic field, measured at four different temperatures for Cu^+:CdSe, Cu^+:InP, and $CuInS_2$ NCs, respectively. For all samples, $\Delta I/I$ increases with increasing magnetic field at all temperatures, and for a given field $\Delta I/I$ generally decreases with increasing temperature. Above ∼1 T, $\Delta I/I$ increases fairly linearly with field at all temperatures, with possible evidence of saturation in the $CuInS_2$ NCs at 2 K. The dashed lines in Figure 5D−F show linear fits of the high-field data with the y-intercept fixed at zero. The observation of temperature-dependent MCPL indicates that this emission originates from excited states with nonzero angular momentum.

$$\frac{\Delta I}{I} = \frac{I_L - I_R}{I_L + I_R} = \frac{\sigma^- - \sigma^+}{\sigma^- + \sigma^+} \quad (1)$$

At the lowest temperatures, all three samples show a small inflection in the MCPL intensity at very low fields (0−1 T, insets to Figure 5D−F) before the field dependence approaches linearity. At higher temperatures, the data become more linear with field in the region between 0 and 1 T. For comparison, the Supporting Information contains MCPL data for a sample of Cu^+:CdSe NCs that exhibits significant intensity of both excitonic and copper-based PL. The excitonic MCPL is negative and its intensity increases linearly with increasing field over the entire field range (0−6 T), consistent with this excitonic PL coming from undoped CdSe NCs.[51] The copper-based MCPL shows the same inflection between 0 and 1 T as seen in Figure 5. This inflection, which is essentially identical to that reported previously from MCPL measurements of $CuInS_2$ and copper-doped ZnSe NCs between 0 and 1 T at 3K,[42] is therefore clearly associated with the presence of copper. These data were previously interpreted in terms of Cu^{2+} in the NC ground state,[42] but similar nonlinearities are observed in the magneto-optics of various copper-doped semiconductors, where they have been attributed to level crossings within an axial zero-field-split triplet spin manifold of the luminescent $ML_{CB}CT$ excited state (very small positive zero-field splittings of $D \sim +0.01$ to $+0.05$ meV).[52,53] This interpretation was supported by optically detected magnetic resonance (ODMR) measurements on oriented single crystals.[52] Although a detailed quantitative analysis of this zero-field splitting in the NCs is beyond the scope of the present study, the nonlinear field dependences observed in the MCPL data of Figure 5 and ref 42 appear to have the same origin as in the bulk samples, and the small magnetic fields at which the inflections occur in Figure 5 are consistent with very small zero-field splittings in the nanocrystals like in bulk. Overall, the remarkably similar MCPL data for all three NC samples at both small and large magnetic fields and as a function of temperature indicate that the basic magnetic properties of the luminescent excited states of these materials are very similar.

■ ANALYSIS

Kinetic Model for Radiative Decay from Singlet and Triplet Excited States. The observation that the PL intensity increases with increasing temperature over the same temperature range (2−60 K) where its lifetime decreases for Cu^+:CdSe, Cu^+:InP, and $CuInS_2$ NCs (Figure 4B) indicates that this lifetime decrease is not due to thermally activated nonradiative decay processes. Rather, we attribute the temperature dependence of the PL lifetimes in all three of these materials to a magnetic-exchange splitting within the luminescent excited state. This excited state involves two distinct spins, that of the delocalized photoexcited electron in the conduction band ($S = 1/2$) and that of the unpaired electron resulting from hole localization at copper ($S = 1/2$). Exchange coupling of these two spins yields singlet and triplet $ML_{CB}CT$ excited states, as illustrated in Figure 6A. For simplicity, Figure 6A shows only the highest-energy 3d orbital of the copper ion; all of the other 3d orbitals are fully occupied in the ground state and both excited states considered here. Analogous singlet−triplet splittings have been observed previously in the luminescent excited states of bulk Cu^+-doped semiconductors[52−55] and molecular Cu^+ coordination complexes.[56−59] In this interpretation, the temperature dependence of the PL lifetime is dictated by the Boltzmann populations of the singlet and triplet excited states, which have very different radiative rate constants. Radiative decay from the triplet excited state is slow because of the spin selection rule, $\Delta S = 0$.

The observation in Figure 4 that the PL lifetimes increase with decreasing temperature below 60 K for all three samples provides a direct experimental indication that the triplet excited states are lower in energy than the singlet excited states in each material, as illustrated in Figure 6B. This conclusion is confirmed by the data in Figure 7, which demonstrate a correlation between the PL lifetime and the MCPL intensity. The MCPL transitions are described schematically on the right side of Figure 6B, neglecting the zero-field splitting of the triplet state. Application of a magnetic field ($B > 0$) splits the emissive triplet state into its three Zeeman components, with σ^- and σ^+ emission allowed from the $m_S = \pm 1$ components at different energies. Boltzmann population differences between these two levels yield nonzero values of $\Delta I/I$. Importantly, the singlet excited state does not split and hence yields no MCPL to first order. MCPL is thus only obtained from triplet-state emission. Increasing the temperature shifts emission from the triplet to the singlet state, shortening the PL decay and concomitantly reducing the MCPL intensity. The correlation

DOI: 10.1021/jacs.5b08547
J. Am. Chem. Soc. 2015, 137, 13138−13147

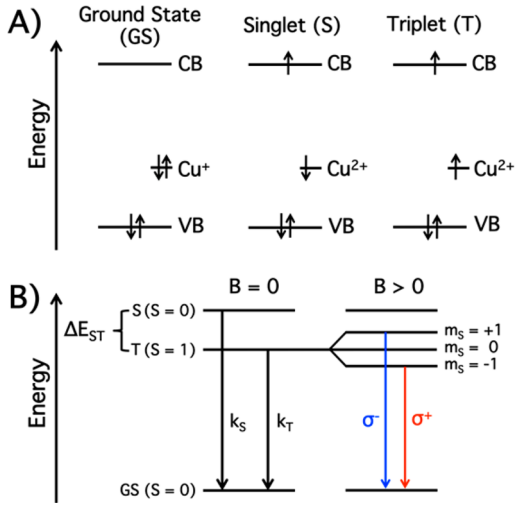

Figure 6. (A) Orbital energy level diagram depicting the ground-state and singlet and triplet luminescent excited-state configurations of a copper-doped semiconductor nanocrystal. "CB" and "VB" denote the lowest- and highest-energy conduction- and valence-band orbitals, respectively. For simplicity, only the highest-energy copper 3*d* orbital is shown. (B) Qualitative energy level diagrams illustrating the energies of the singlet and triplet excited states from (A) and their splitting in an applied magnetic field ($B > 0$). The zero-field ($B = 0$) diagram illustrates the parameters used in eq 2 and eq 3, where k_S and k_T indicate rate constants for decay to the ground state from the singlet and triplet excited states, respectively, and ΔE_{ST} represents the singlet–triplet splitting energy. The $B > 0$ diagram illustrates the Zeeman splitting of the triplet excited state that gives rise to MCPL intensity.

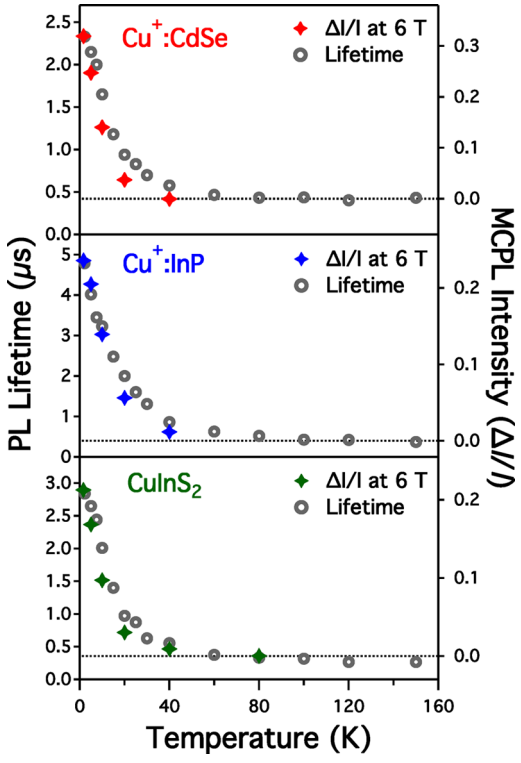

Figure 7. MCPL intensities (6 T, closed crosses) and PL lifetimes (0 T, open circles) plotted versus temperature for Cu^+:CdSe (red), Cu^+:InP (blue), and $CuInS_2$ (green) NCs. Data points taken from the data in Figures 4 and 5.

between the MCPL intensity and the PL lifetime in Figure 7 confirms the interpretation of the data from both experiments in terms of singlet–triplet splittings.

The zero-field diagram in Figure 6B can now be used to model the temperature dependence of the PL decay shown in Figure 4B and Figure 7. Here, k_S and k_T represent the overall rate constants for decay (radiative + nonradiative) from the singlet and triplet excited states, respectively. For simplicity, we assume negligible temperature-dependent nonradiative decay for both states within this temperature window (2–150 K), justified by the relatively constant integrated PL intensity across this range. Interconversion between the singlet and triplet excited states is assumed to be fast relative to decay to the ground state,[55,58,60] which allows the singlet and triplet excited-state populations to be in thermal quasi-equilibrium during decay. The temperature dependence of the PL lifetime, τ_{PL}, is then given by eq 2, where ΔE_{ST} is the energy difference between the singlet and triplet excited states, and k_B is Boltzmann's constant.

$$\tau_{PL}(T, \Delta E_{ST}) = \frac{1 + 3\exp(\Delta E_{ST}/k_B T)}{k_S + 3k_T\exp(\Delta E_{ST}/k_B T)} \quad (2)$$

Eq 2 has been used previously to describe the temperature dependence of excited-state lifetimes in bulk Cu^+-doped semiconductors and in molecular Cu^+ coordination complexes that have singlet and triplet charge-transfer excited states.[54−57] In the low-temperature limit ($k_BT \ll \Delta E_{ST}$) eq 2 predicts that the PL lifetime should approach the lifetime of the triplet state ($\tau_T = 1/k_T$), whereas in the high-temperature limit ($k_BT \gg \Delta E_{ST}$) eq 2 predicts that the PL lifetime should approach $\tau_{PL} = 4/k_S$, because $k_S \gg k_T$. Our experimental lifetimes do reach constant values at high temperatures (Figure 4B and Figure S6), indicating that we have reached the high-temperature limit of eq 2 for each sample. No clear low-temperature plateau is observed in the data of Figure 4B, however. Although this behavior could indicate very small values of ΔE_{ST}, fits of the data to eq 2 are inadequate, showing exaggerated curvature not observed experimentally (see Supporting Information). These poor fits suggest that a distribution of ΔE_{ST} exists within the NC ensemble that is not described by eq 2. To a first approximation, this distribution arises from the distribution in radial positions of the copper-bound holes within the ensemble of photoexcited NCs. The magnitude of ΔE_{ST} in a particular NC is determined by the strength of the exchange coupling between the conduction-band electron and the unpaired electron on the Cu^{2+}-like ion, which in turn depends on the spatial overlap between these two spins. In these quantum-confined NCs, conduction-band electrons can be approximated as particles in a spherical well. The amplitude of the wave function for an electron in the lowest-energy conduction band orbital ($1S_e$) is greatest at the NC center and decreases with increasing radial displacement from the center. A nanocrystal with the copper-bound hole in its precise center will thus have a larger ΔE_{ST} than one with the copper-bound hole near its surface. Additionally, because the envelope function describing the lowest-energy VB hole is also S-like, and because the probability of hole localization to a particular Cu^+ site also depends on exchange interactions between the VB hole and the Cu^+,[61] NCs containing more than one Cu^+ dopant will preferentially show luminescence from copper dopants nearer to the NC center.

DOI: 10.1021/jacs.5b08547
J. Am. Chem. Soc. 2015, 137, 13138−13147

Eq 3 extends eq 2 to account for the distribution in ΔE_{ST} described above. In eq 3, $\Delta E_{ST,avg}$ is the average value of ΔE_{ST} for the NC ensemble, $\Delta E_{ST}(r)$ is the value of ΔE_{ST} for an excited NC in which the copper-bound hole is located at a distance r from the NC center, n is the total number of cations per QD, N_0 is the cation density, R is the NC radius, and $|\psi(r)|^2$ describes the probability density of an electron (hole) in the lowest-energy orbital of the conduction (valence) band. The Supporting Information contains the details of the derivation of eq 3, in which we assume that it is equally probable to find a Cu^+ ion at any location within the ground-state NC, and that, for NCs containing multiple Cu^+ ions (e.g., $CuInS_2$), the probability of hole trapping at a particular Cu^+ is proportional to the probability density of the initial photogenerated hole at that location. For doped NCs that contain only one Cu^+, the probability density of the photogenerated hole does not impact the radial position of the localized hole in the excited state. Table 2 reports the values of $\Delta E_{ST,avg}$ and k_T obtained from fits

Table 2. Parameters from Fitting of PL Lifetime Temperature Dependence to Eq 3

sample	k_S (s^{-1})[a]	k_T (s^{-1})	$\Delta E_{ST,avg}$ (meV)
Cu^+:CdSe	9.4×10^6	3.8×10^5	0.85
Cu^+:InP	9.2×10^6	2.0×10^5	1.3
$CuInS_2$	1.4×10^7	3.1×10^5	1.1

[a]Fixed parameter.

of the data in Figure 4B to eq 3. A simpler model that neglects the initial hole probability density yields similar $\Delta E_{ST,avg}$ values (1.8 and 2.7 meV for Cu^+:CdSe and Cu^+:InP, respectively). Both models yield small $\Delta E_{ST,avg}$ values, and we consider their difference to be within the uncertainty of the measurement. Importantly, in the high-temperature limit ($k_BT \gg \Delta E_{ST}(r)$ for all $0 < r < R$), eq 3a reduces to eq 2, and therefore still predicts that τ_{PL} approaches $4/k_S$. The solid lines in Figure 4B are fits of the data to eq 3 in which k_S was fixed to $4/\tau_{PL}$(high-T), where τ_{PL}(high-T) is the average of the experimental PL lifetimes measured between 80 and 150 K for that sample.

$$\tau_{PL}(T) = \int_0^R 4\pi r^2 |\psi(r)|^2 \frac{1 + 3\exp(\Delta E_{ST}(r)/k_BT)}{k_S + 3k_T\exp(\Delta E_{ST}(r)/k_BT)}\, dr \quad (3a)$$

$$\Delta E_{ST}(r) = \frac{n\Delta E_{ST,avg}}{N_0}|\psi(r)|^2 \quad (3b)$$

$$|\psi(r)|^2 = \frac{\sin^2\left(\frac{\pi r}{R}\right)}{2\pi R r^2} \quad (3c)$$

Notably, the values of $\Delta E_{ST,avg}$ obtained for Cu^+:CdSe, Cu^+:InP, and $CuInS_2$ are quantitatively very similar (each is ~1 meV), further validating the assertion that the mechanism of PL in $CuInS_2$ NCs is the same as that in the Cu^+-doped semiconductor NCs, involving recombination of a delocalized conduction-band electron with a localized copper-bound hole. The values for $\Delta E_{ST,avg}$ reported here are similar in magnitude to excited-state singlet−triplet splittings reported for luminescent copper defects in bulk GaP, most of which range from ~0.7−8.0 meV depending on the specific copper defect.[55] One copper defect in GaP has a very large binding energy (i.e., highly localized carriers) and a singlet−triplet splitting of ~90 meV,[52,55] which is more similar to splittings reported for luminescent Cu^+ molecular complexes (90−140 meV).[56,59,62] These large singlet−triplet splittings are a consequence of the relatively localized electron and hole wave functions in the molecules. Overall, the small singlet−triplet splittings reported in Table 2 are consistent with radiative recombination of a delocalized conduction-band electron and a copper-localized hole.

DISCUSSION

Exciton Self-Trapping in $CuInS_2$ Nanocrystals. Under every experimental condition probed here, the PL of the $CuInS_2$ NCs is essentially indistinguishable from that of the Cu^+-doped CdSe and InP NCs. All three NCs show essentially the same PL line widths, Stokes shifts, and manifestations of excited-state singlet−triplet and zero-field splittings in their PL and MCPL temperature dependence. The lowest-energy excited states detectable by absorption spectroscopy also appear similar. These similarities strongly implicate similar electronic structures of the luminescent excited states in these NCs.

In the Cu^+-doped NCs, the luminescence mechanism is understood to involve $ML_{CB}CT$ recombination (Figure 1), and is closely analogous to that of the corresponding bulk materials. In bulk $CuInS_2$, PL is associated with midgap trap states linked to particular point defects: Cu_{In}, V_{In}, and V_{Cu}.[35,36] To date, $CuInS_2$ NC PL has also been interpreted in terms of defects.[3,5,37−41] Direct comparison shows that the "broad" deep-trap PL of bulk $CuInS_2$ is in fact substantially sharper (fwhm ~30 meV)[35] than the $CuInS_2$ NC PL (fwhm ~360 meV), however, suggesting that the emissive excited state in the $CuInS_2$ NCs may exhibit stronger electron−phonon coupling than that in bulk $CuInS_2$.

From the data presented here, we propose that the emissive excited state of $CuInS_2$ NCs is *fundamentally* different from that of bulk $CuInS_2$. Specifically, we propose that the $CuInS_2$ NC PL does not arise from point defects as in bulk, but instead results from exciton self-trapping (Figure 8).[43−46] Self-trapped excitons form when electron−phonon coupling energies are large relative to carrier delocalization (resonance) energies, generating positive feedback between carrier contraction and stabilization.[44] Typically, electron−phonon coupling is significant for only one of the two photogenerated carriers, and that would be the hole in the case of $CuInS_2$ NCs. Cu^+ ions typically exhibit large nuclear reorganization energies when oxidized, associated with large low-symmetry (Jahn−Teller) nuclear distortions that stabilize the added hole. MLCT excited-state nuclear reorganization energies of ~0.25−0.4 eV have been reported for Cu^+ molecular complexes, for example.[60,63] Exciton self-trapping is well-known in AgCl, which also involves a d^{10} lattice cation that undergoes a Jahn−Teller distortion to localize a hole, generating a broad PL band and a large Stokes shift.[44,45]

In $CuInS_2$ NCs, excited states that involve delocalized holes will be subject to nuclear fluctuations that modulate the hole potential substantially. Hole contraction in response to this modulation enhances the nuclear distortion, causing further hole localization, etc., until a new equilibrium geometry is reached that corresponds to a highly contracted hole localized about a distorted lattice copper ion. The precise time scale of hole localization is unknown, but it could be as fast as the vibrational cooling (femto- to few picoseconds). In this way, the luminescence of $CuInS_2$ NCs involves a delocalized CB electron recombining with a deeply copper-localized hole

DOI: 10.1021/jacs.5b08547
J. Am. Chem. Soc. 2015, 137, 13138−13147

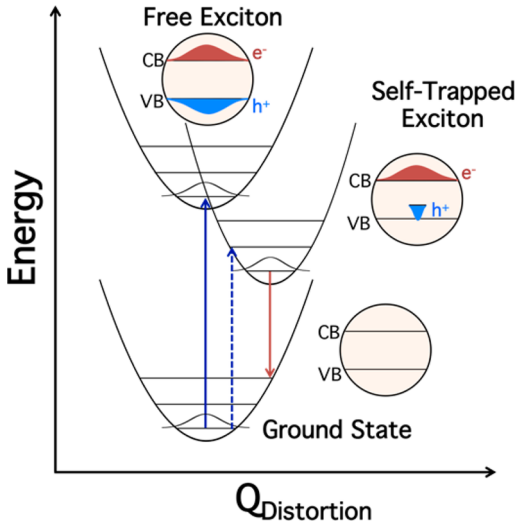

Figure 8. Qualitative single-configurational-coordinate diagram illustrating absorption, exciton self-trapping, and luminescence in $CuInS_2$ nanocrystals. Photoexcitation (solid blue arrow) excites a $CuInS_2$ nanocrystal from its ground state to a delocalized excitonic state. This delocalized excitonic state rapidly relaxes to a self-trapped excitonic state via hole localization mediated by strong vibronic coupling and a resulting nuclear distortion at the copper. Luminescence from this self-trapped excitonic state to the ground state (solid red arrow) is characterized by a large Stokes shift and a vibronically broadened band shape. Direct excitation of the self-trapped excitonic state (dashed blue arrow) is observed as a comparably broad, low-extinction "foot" in the absorption spectrum.

(Figure 8), precisely analogous to the luminescent excited states of Cu^+-doped II–VI and III–V semiconductors. This parallel is manifested in similar PL band shapes, which in both classes of materials primarily reflect the nuclear reorganization associated with hole trapping at copper, and in similar ΔE_{ST}, reflecting similar electron–hole spatial overlap. The assignment of $CuInS_2$ PL to self-trapped excitons is supported by the similar per-copper extinction coefficients of the first absorption band in $CuInS_2$ NCs and the sub-bandgap "foot" in the Cu^+:CdSe and Cu^+:InP NCs (Figure 3). These low-extinction features are assigned as direct excitation of the $ML_{CB}CT$ excited state in the Cu^+:CdSe and Cu^+:InP NCs, and direct excitation of self-trapped excitons in the $CuInS_2$ NCs (dashed arrow in Figure 8). This assignment is also consistent with the temperature dependence of the $CuInS_2$ NC PL line width (see Supporting Information),[39] which could be interpreted in terms of vibronic hot bands. The proposal of exciton self-trapping in $CuInS_2$ NCs is therefore consistent with all of the experimental observations reported in this manuscript. Importantly, this mechanism identifies the hole trap in $CuInS_2$ NCs as a lattice copper, and does not invoke other point defects. We note that the PL spectrum of $Cu_{1-x}InS_2$ NCs ($0 < x < 0.8$) appears similar to that of stoichiometric $CuInS_2$ NCs,[40] which may suggest that exciton self-trapping is competitive even in the presence of nonstoichiometries and other compositional defects.

An interesting question pertains to why self-trapped excitons dominate the PL of $CuInS_2$ NCs but not the PL of bulk $CuInS_2$. A compelling hypothesis would be that the small volumes of luminescent $CuInS_2$ NCs do not offer sufficient resonance energies to outcompete self-trapping. In other words, the kinetic energy favoring hole delocalization is smaller than the potential energy favoring hole localization. This hypothesis predicts that the stability of the $CuInS_2$ self-trapped exciton relative to the delocalized exciton should decrease with increasing NC volume until the energies of these two states cross and the material reverts to bulk-like behavior. Future experiments will be aimed at testing this possibility and probing deeper into the characteristics of these self-trapped excitons in $CuInS_2$ NCs.

CONCLUSIONS

In summary, the optical and magneto-optical properties of the luminescent excited state of $CuInS_2$ NCs are essentially identical to those of the luminescent excited states in Cu^+:CdSe and Cu^+:InP NCs. All three of these materials exhibit broad PL line widths and large Stokes shifts (Figure 2, Table 1), quantitatively similar magnetic-exchange splittings between singlet and triplet excited states (Figure 4, Table 2), similar first absorption features (Figure 3), and similar zero-field splittings of their triplet excited states (Figure 5). We therefore conclude that the mechanism of PL in $CuInS_2$ NCs is the same as that in Cu^+-doped semiconductor NCs, involving charge-transfer recombination of a CB electron with a hole that is strongly localized at a Cu^+ site. This conclusion implies that the PL mechanism in $CuInS_2$ NCs is different from that of bulk $CuInS_2$, and leads us to propose that the luminescent excited state of $CuInS_2$ NCs is a self-trapped exciton (Figure 8). The fundamental insights into the luminescence of copper-doped and copper-based NCs gained from the measurements presented here will help to advance the development of such NCs as colloidal phosphors for applications as diverse as solution-processed luminescent solar concentrators and liquid-phase nanoimaging.

ASSOCIATED CONTENT

Supporting Information

The Supporting Information is available free of charge on the ACS Publications website at DOI: 10.1021/jacs.5b08547.

Additional PL and structural characterization data, MCD spectra, and derivation of eq 3. (PDF)

AUTHOR INFORMATION

Corresponding Author

*gamelin@chem.washington.edu

Notes

The authors declare no competing financial interest.

ACKNOWLEDGMENTS

Support from the Department of Energy (Energy Efficiency and Renewable Energy postdoctoral research award to K.E.K.) and the National Science Foundation (DMR-1505901 to D.R.G. and Graduate Research Fellowship DGE-1256082 to H.D.N.) is gratefully acknowledged. Additional fellowship support was provided by the Clean Energy Institute at the University of Washington (to T.B.K.)

REFERENCES

(1) Yen, W. M.; Shionoya, S.; Yamamoto, H. *Phosphor Handbook*, 2nd ed.; CRC Press: Boca Raton, FL, 2007.

(2) Suyver, J. F.; van der Beek, T.; Wuister, S. F.; Kelly, J. J.; Meijerink, A. *Appl. Phys. Lett.* **2001**, *79*, 4222–4224.

(3) Li, L.; Pandey, A.; Werder, D. J.; Khanal, B. P.; Pietryga, J. M.; Klimov, V. I. *J. Am. Chem. Soc.* **2011**, *133*, 1176–1179.

DOI: 10.1021/jacs.5b08547
J. Am. Chem. Soc. 2015, 137, 13138–13147

(4) Allen, P. M.; Bawendi, M. G. *J. Am. Chem. Soc.* **2008**, *130*, 9240−9241.
(5) Zhong, H.; Bai, Z.; Zou, B. *J. Phys. Chem. Lett.* **2012**, *3*, 3167−3175.
(6) Kolny-Olesiak, J.; Weller, H. *ACS Appl. Mater. Interfaces* **2013**, *5*, 12221−12237.
(7) Aldakov, D.; Lefrançois, A.; Reiss, P. *J. Mater. Chem. C* **2013**, *1*, 3756−3776.
(8) Grandhi, G. K.; Tomar, R.; Viswanatha, R. *ACS Nano* **2012**, *6*, 9751−9763.
(9) Xie, R.; Peng, X. *J. Am. Chem. Soc.* **2009**, *131*, 10645−10651.
(10) Nose, K.; Omata, T.; Otsuka-Yao-Matsuo, S. *J. Phys. Chem. C* **2009**, *113*, 3455−3460.
(11) Xie, R.; Rutherford, M.; Peng, X. *J. Am. Chem. Soc.* **2009**, *131*, 5691−5697.
(12) Xu, S.; Wang, C.; Wang, Z.; Zhang, H.; Yang, J.; Xu, Q.; Shao, H.; Li, R.; Lei, W.; Cui, Y. *Nanotechnology* **2011**, *22*, 275605.
(13) Song, W.-S.; Yang, H. *Appl. Phys. Lett.* **2012**, *100*, 183104.
(14) Bradshaw, L. R.; Knowles, K. E.; McDowall, S.; Gamelin, D. R. *Nano Lett.* **2015**, *15*, 1315−1323.
(15) Knowles, K. E.; Kilburn, T. B.; Alzate, D. G.; McDowall, S.; Gamelin, D. R. *Chem. Commun.* **2015**, *51*, 9129−9132.
(16) While this manuscript was under review, the following manuscript was published online: Meinardi, F.; McDaniel, H.; Carulli, F.; Colombo, A.; Velizhanin, K. A.; Makarov, N. S.; Simonutti, R.; Klimov, V. I.; Brovelli, S. *Nat. Nanotechnol.* **2015**, DOI: 10.1038/nnano.2015.178.
(17) Suzuki, A.; Shionoya, S. *J. Phys. Soc. Jpn.* **1971**, *31*, 1455−1461.
(18) Grandhi, G. K.; Viswanatha, R. *J. Phys. Chem. Lett.* **2013**, *4*, 409−415.
(19) Srivastava, B. B.; Jana, S.; Pradhan, N. *J. Am. Chem. Soc.* **2011**, *133*, 1007−1015.
(20) Zhang, W.; Lou, Q.; Ji, W.; Zhao, J.; Zhong, X. *Chem. Mater.* **2014**, *26*, 1204−1212.
(21) Pradhan, N.; Goorskey, D.; Thessing, J.; Peng, X. *J. Am. Chem. Soc.* **2005**, *127*, 17586−17587.
(22) Whitham, P. J.; Knowles, K. E.; Reid, P. J.; Gamelin, D. R. *Nano Lett.* **2015**, *15*, 4045−4051.
(23) Brovelli, S.; Galland, C.; Viswanatha, R.; Klimov, V. I. *Nano Lett.* **2012**, *12*, 4372−4379.
(24) Buckner, M. T.; McMillin, D. R. *J. Chem. Soc., Chem. Commun.* **1978**, 759−761.
(25) Everly, R. M.; Ziessel, R.; Suffert, J.; McMillin, D. R. *Inorg. Chem.* **1991**, *30*, 559−561.
(26) Felder, D.; Nierengarten, J.-F.; Barigelletti, F.; Ventura, B.; Armaroli, N. *J. Am. Chem. Soc.* **2001**, *123*, 6291−6299.
(27) Meulenberg, R. W.; van Buuren, T.; Hanif, K. M.; Willey, T. M.; Strouse, G. F.; Terminello, L. J. *Nano Lett.* **2004**, *4*, 2277−2285.
(28) Jawaid, A. M.; Chattopadhyay, S.; Wink, D. J.; Page, L. E.; Snee, P. T. *ACS Nano* **2013**, *7*, 3190−3197.
(29) Tang, A.; Yi, L.; Han, W.; Teng, F.; Wang, Y.; Hou, Y.; Gao, M. *Appl. Phys. Lett.* **2010**, *97*, 033112.
(30) Gul, S.; Cooper, J. K.; Corrado, C.; Vollbrecht, B.; Bridges, F.; Guo, J.; Zhang, J. Z. *J. Phys. Chem. C* **2011**, *115*, 20864−20875.
(31) Isarov, A. V.; Chrysochoos, J. *Langmuir* **1997**, *13*, 3142−3149.
(32) Corrado, C.; Jiang, Y.; Oba, F.; Kozina, M.; Bridges, F.; Zhang, J. Z. *J. Phys. Chem. A* **2009**, *113*, 3830−3839.
(33) Bol, A. A.; Ferwerda, J.; Bergwerff, J. A.; Meijerink, A. *J. Lumin.* **2002**, *99*, 325−334.
(34) Viswanatha, R.; Brovelli, S.; Pandey, A.; Crooker, S. A.; Klimov, V. I. *Nano Lett.* **2011**, *11*, 4753−4758.
(35) Binsma, J. J. M.; Giling, L. J.; Bloem, J. *J. Lumin.* **1982**, *27*, 35−53.
(36) Ueng, H. Y.; Hwang, H. L. *J. Phys. Chem. Solids* **1989**, *50*, 1297−1305.
(37) Castro, S. L.; Bailey, S. G.; Raffaelle, R. P.; Banger, K. K.; Hepp, A. F. *J. Phys. Chem. B* **2004**, *108*, 12429−12435.
(38) Tran, T. K. C.; Le, Q. P.; Nguyen, Q. L.; Li, L.; Reiss, P. *Adv. Nat. Sci.: Nanosci. Nanotechnol.* **2010**, *1*, 025007.
(39) Shi, A.; Wang, X.; Meng, X.; Liu, X.; Li, H.; Zhao, J. *J. Lumin.* **2012**, *132*, 1819−1823.
(40) Kim, Y.-K.; Ahn, S.-H.; Chung, K.; Cho, Y.-S.; Choi, C.-J. *J. Mater. Chem.* **2012**, *22*, 1516−1520.
(41) Sun, J.; Ikezawa, M.; Wang, X.; Jing, P.; Li, H.; Zhao, J.; Masumoto, Y. *Phys. Chem. Chem. Phys.* **2015**, *17*, 11981−11989.
(42) Rice, W. D.; McDaniel, H.; Klimov, V. I.; Crooker, S. A. *J. Phys. Chem. Lett.* **2014**, *5*, 4105−4109.
(43) Mott, N. F.; Stoneham, A. M. *J. Phys. C: Solid State Phys.* **1977**, *10*, 3391−3398.
(44) Toyozawa, Y. *J. Lumin.* **1981**, *24*, 23−30.
(45) Vogelsang, H.; Husberg, O.; Köhler, U.; von der Osten, W.; Marchetti, A. P. *Phys. Rev. B: Condens. Matter Mater. Phys.* **2000**, *61*, 1847−1852.
(46) Song, K. S.; Williams, R. T. *Self-Trapped Excitons*, 2nd ed.; Springer-Verlag: New York, 1996.
(47) Tananaev, P. N.; Dorofeev, S. G.; Vasil'ev, R. B.; Kuznetsova, T. A. *Inorg. Mater.* **2009**, *45*, 347−351.
(48) Piepho, S. B.; Schatz, P. N. *Group Theory in Spectroscopy: With Applications to Magnetic Circular Dichroism*; Wiley: New York, 1983.
(49) Yu, W. W.; Qu, L.; Guo, W.; Peng, X. *Chem. Mater.* **2003**, *15*, 2854−2860.
(50) Mićić, O. I.; Ahrenkiel, S. P.; Nozik, A. J. *Appl. Phys. Lett.* **2001**, *78*, 4022−4024.
(51) Beaulac, R.; Archer, P. I.; Liu, X.; Lee, S.; Salley, G. M.; Dobrowolska, M.; Furdyna, J. K.; Gamelin, D. R. *Nano Lett.* **2008**, *8*, 1197−1201.
(52) Gislason, H. P.; Monemar, B.; Dean, P. J.; Herbert, D. C.; Depinna, S.; Cavenett, B. C.; Killoran, N. *Phys. Rev. B: Condens. Matter Mater. Phys.* **1982**, *26*, 827−845.
(53) Kana-ah, A.; Cavenett, B. C.; Gislason, H. P.; Monemar, B.; Pistol, M. E. *J. Phys. C: Solid State Phys.* **1986**, *19*, 1239−1250.
(54) Bergman, P.; Monemar, B. *J. Lumin.* **1987**, *38*, 87−89.
(55) Bergman, P.; Monemar, B.; Pistol, M.-E. *Phys. Rev. B: Condens. Matter Mater. Phys.* **1989**, *40*, 12280−12289.
(56) Blasse, G.; McMillin, D. R. *Chem. Phys. Lett.* **1980**, *70*, 1−3.
(57) Kirchhoff, J. R.; Gamache, R. E., Jr.; Blaskie, M. W.; Del Paggio, A. A.; Lengel, R. K.; McMillin, D. R. *Inorg. Chem.* **1983**, *22*, 2380−2384.
(58) Everly, R. M.; McMillin, D. R. *J. Phys. Chem.* **1991**, *95*, 9071−9075.
(59) Leitl, M. J.; Krylova, V. A.; Djurovich, P. I.; Thompson, M. E.; Yersin, H. *J. Am. Chem. Soc.* **2014**, *136*, 16032−16038.
(60) Iwamura, M.; Watanabe, H.; Ishii, K.; Takeuchi, S.; Tahara, T. *J. Am. Chem. Soc.* **2011**, *133*, 7728−7736.
(61) Beaulac, R.; Feng, Y.; May, J. W.; Badaeva, E.; Gamelin, D. R.; Li, X. *Phys. Rev. B: Condens. Matter Mater. Phys.* **2011**, *84*, 195324.
(62) Hofbeck, T.; Monkowius, U.; Yersin, H. *J. Am. Chem. Soc.* **2015**, *137*, 399−404.
(63) Waterland, M. R.; Howell, S. L.; Gordon, K. C.; Burrell, A. K. *J. Phys. Chem. A* **2005**, *109*, 8826−8833.

DOI: 10.1021/jacs.5b08547
J. Am. Chem. Soc. 2015, 137, 13138−13147